A Hippocampal-Entorhinal Cortex Neuronal Network for Dynamical Mechanisms of Epileptic Seizure

Ying Yu, Fang Han, and Qingyun Wang

***Abstract*— Temporal lobe epilepsy (TLE) is thought to be associated with neuronal hyperexcitability in the hippocampal-entorhinal cortical (EC) circuit. Due to the complexity of the hippocampal-EC network connections, the biophysical mechanisms of the different circuits in epilepsy generation and propagation are still not fully established. In this work, we propose a hippocampal-EC neuronal network model to explore the mechanism of epileptic generation. We demonstrate that enhanced excitability of pyramidal neurons in cornu ammonis 3 (CA3) can drive hippocampal-EC to produce a transition from background to seizure state and cause exaggerated phase-amplitude coupling (PAC) phenomenon of theta modulated high-frequency oscillations (HFO) in CA3, cornu ammonis 1 (CA1), dentate gyrus, and EC. Interestingly, PAC strength indirectly responds to the degree of CA3 pyramidal (PY) neuron hyperexcitability, suggesting that PAC can be used as a potential marker of seizures. Furthermore, we find that enhanced synaptic connectivity of mossy cells to granule cells and CA3 PY neurons drives the system to produce epileptic discharges. These two channels may play a key role in mossy fiber sprouting. In particular, the PAC phenomenon of delta-modulated HFO and theta-modulated HFO can be generated according to the different degrees of moss fiber sprouting. Finally, the results suggest that hyperexcitability of stellate cells in EC can lead to seizures, which supports the argument that EC can act as an independent source of seizures. Overall, these results highlight the key role of different circuits in seizures, providing a theoretical basis and new insights into the generation and propagation of TLE.**

***Index Terms*— Computational model, temporal lobe epilepsy, dynamical transition, hippocampal-entorhinal cortical network.**

Manuscript received 4 October 2022; revised 20 February 2023; accepted 17 March 2023. Date of publication 7 April 2023; date of current version 12 April 2023. This work was supported in part by the National Natural Science Foundation of China under Grant 11932003, Grant 11972115, Grant 12272092, and Grant 12202027; and in part by the China Postdoctoral Science Foundation under Grant 2021TQ0025. *(Corresponding authors: Fang Han; Qingyun Wang.)*

Ying Yu is with the School of Engineering Medicine, Beihang University, Beijing 100191, China.

Fang Han is with the College of Information Science and Technology, Donghua University, Shanghai 201620, China (e-mail: yadiahan@dhu.edu.cn).

Qingyun Wang is with the Department of Dynamics and Control, Beihang University, Beijing 100191, China, and also with the Beijing Institute of Brain Disorders, Capital Medical University, Beijing 100069, China (e-mail: nmqingyun@163.com).

This article has supplementary downloadable material available at https://doi.org/10.1109/TNSRE.2023.3265581, provided by the authors.

Digital Object Identifier 10.1109/TNSRE.2023.3265581

I. Introduction

TEMPORAL lobe epilepsy (TLE) is common focal epilepsy, which is closely related to the abnormal neuronal activities of neural networks in the limbic system, such as hippocampus, amygdala, and entorhinal cortex (EC) [1], [2], [3]. The pathological features of TLE include hippocampal sclerosis or Ammon's horn sclerosis, which is accompanied by cell loss [4]. Furthermore, TLE can also cause different morphological changes in hippocampus. A common anatomical feature of TLE is the mossy fibers sprouting, producing abnormal intercellular connections in the dentate gyrus (DG) [5], [6]. The granule cells (GC) of the hippocampal DG are generally considered to be sparsely discharged, whereas GC may be hyperactivated under TLE, leading to hyperexcitability and hypersynchronization in the neural circuits [7]. Recently, Botterill et al. found that mossy cells (MC) excitation of GCs increases, and inhibiting MC activity can reduce seizures [8]. The axons of CA3 pyramidal cells in epileptic rats have also been shown to sprout significantly, forming a denser CA3 to CA3 excitatory connection [9]. In addition, the role of the entorhinal cortex (EC) in epilepsy has also attracted extensive attention. Previous studies have shown that both epileptic rats and TLE patients exhibit preferential loss of EC neurons, suggesting that EC may be a potential candidate for the generation and transmission of TLE [10]. Armstrong et al. found that after kainic acid-induced seizures, there were repeated excitatory connections between the principal cells in layer II of the medial EC [11]. The clinical and experimental evidence suggests that hippocampus and EC may be two independent origins of epileptic activity [3], [12]. It is thus evident that hippocampal-EC neural circuit abnormalities in epileptic seizures take various forms, and the mechanisms of epileptogenesis, including its propagation pathways and activity patterns, are still incompletely understood.

Different regions of the brain in the TLE state show abnormal oscillations at both the neuronal level and the population level [13]. Epileptiform discharges lasting several seconds with tonic and clonic components are found in combined hippocampal-EEG slices from epileptic rats [3]. In addition, high-frequency oscillations (HFO, i.e. ripples at 80-200 Hz and fast ripples at 250-500 Hz) are also present during seizures [14], [15]. Studies have shown that the incidence of HFO is higher in seizure areas, and the location of brain

resection in clinical surgery is closely related to the area of HFO production [16]. Recent studies show that the HFO may be modulated by low-frequency oscillations. Cross-frequency coupling between different neural signal oscillatory components may serve as markers of epileptic signals [17], [18]. Guirgis et al. found that the modulation intensity of delta oscillations (2-4 Hz) and HFO could more accurately localize the epileptogenic zone in patients [19]. Phase amplitude coupling (PAC) has also been used to identify seizure sites in children with focal epilepsy, and Nonoda et al. suggested that epileptogenic HFOs may be coupled with 3-4 Hz more preferentially than 0.5-1Hz [20]. Samiee explored the PAC between the slow oscillatory phase (slow waves in the -band: 0.18-4 Hz) and the faster rhythm amplitude (-ripple band) in the pilocarpine animal model [21]. They found a strong correlation between PAC signal markers and seizure activity. Therefore, PAC may reflect the pathological network activity of epilepsy initiation and seizure onset. Although HFO has received a lot of attention from scholars, the mechanism of HFO generation is not fully understood yet. The specific generation mechanism of the PAC phenomenon deserves further investigation.

Seizures involve an extraordinarily complex dynamic system composed of multiple regions of the brain. Computational modeling can provide tools to further understand epilepsy pathogenesis and explore new strategies to suppress seizure oscillations [13], [33]. The CA3 and CA1 regions of the hippocampus are thought to be closely associated with various neurological disorders, and modeling the dynamics of the CA3 and CA1 regions is critical to understanding hippocampal function. Demont-Guignard et al. reported a two-compartment model of CA1 pyramidal neurons designed using the Hodgkin-Huxley form and then built a CA1 subfield network, showing that epileptic discharges are generated by synchronous firing of pyramidal cells [22]. Pinsky and Rinzel created a two-compartment model of CA3 that captures the complex firing characteristics of CA3 pyramidal cells [23]. Neymotin et al. constructed a CA3 network model consisting of pyramidal (PY) cells, basket (BS) cells, and oriens-lacunosum moleculare (OLM) cells [24], which was subsequently used to explore the role of hippocampal CA3 subfield neuronal connectivity in the generation of epileptiform activity [25]. Some models of CA3-CA1 coupling were also developed to study signal transitions and the sharp wave-ripple complex in the hippocampal CA3-CA1 region [27], [41]. TLE also causes many different morphological changes in the granule cells of the DG. There are a number of computational models of DG that explore the effects of morphological changes in epileptic state [45], [46]. For example, a detailed model of DG neuronal networks was proposed to investigate the effects of mossy fiber germination and mossy cell loss on DG neuronal activity [26]. They found that low levels of mossy fiber sprouting also caused an increase in dentate excitability. In addition, Some multi-regional coupled models of hippocampus and EC have also been developed in recent years. For example, the DG-CA3 network model was developed to study the transitions of seizure discharge [28]. Sora Ahn et al. proposed a CA1-CA3-DG-EC network, which replicates the three activities of fast interictal discharges, slow interictal discharges, and ictal discharges in epileptic seizures [30]. However, in this network model, the modeling methods of different regions are consistent, lacking the specificity of neurons between regions.

As shown above, modeling analysis provides a useful tool in the study of the epileptogenic mechanisms of TLE. The modeling of the different loops for the hippocampal region is relatively clear, but the transmission of abnormal epileptic oscillations throughout the hippocampal-EC loop is not fully understood. To understand more deeply the mechanisms of TLE generation and propagation in the hippocampal-EC system, an integrated network model dominated by neuronal diversity is required. Therefore, we develop a hippocampal-EC neuronal network model to explore the underlying mechanisms of epilepsy generation. The model consists of four regions, CA1, CA3, EC, and DG, including CA1 PY neurons, CA3 PY neurons, EC layer V PY neurons, EC layer II stellate cells (SC), GCs, MCs, and two types of interneurons. Connections between different regions are based on a physiological structural basis. Based on the detailed neuronal network model, we analyze three potential mechanisms of seizure generation, which are closely related to PY neurons in CA3, MCs in DG, and SCs in EC. The transition of the system from the background state to the two types of epileptic states is achieved by adjusting the key parameters within the different loops. Besides, we also explore the PAC phenomenon of low-frequency theta oscillation modulating HFO in the epileptic seizure state. These findings clearly outline the possible mechanisms of epileptic seizures in the hippocampal-EC circuit, further reproducing synchronized oscillations, HFO, and PAC phenomena in epileptic discharges in clinical studies and animal experiments.

II. Models and Methods

A. CA3 and CA1 Circuits

We use the CA3 network model proposed by Neymotin et al [31], which consists of 200 five-compartment PY neurons, 50 one-compartment BS interneurons, and 50 one-compartment OLM interneurons. Consistent with previous studies [31], [32], PY neurons include one basal dendrite, one soma, and three apical dendrites (Adend1, Adend2, and Adend3). The membrane dynamics equations of different neurons are as follows:

$$C_m \frac{dV_{PY}}{dt} = -I_{Na} - I_{Kdr} - I_L - I_{KA} - I_h - I_{syn} + I_{app-PY} \tag{1}$$

$$C_m \frac{dV_{BS}}{dt} = -I_{Na} - I_{Kdr} - I_L - I_{syn} + I_{app-BS} \tag{2}$$

$$C_m \frac{dV_{OLM}}{dt} = -I_{Na} - I_{Kdr} - I_L - I_{KCa} - I_h - I_{syn} + I_{app-OLM} \tag{3}$$

where V_{PY}, V_{BS} and V_{OLM} are the membrane potentials of the PY, BS, and OLM neurons, respectively. The equations are the same for all compartments of PY, but the parameters are slightly different. C_m is the membrane capacitance. All neurons contain leak current I_L, sodium current I_{Na}, and delayed

rectifier current I_{Kdr}. For PY neuron, it also includes A-type potassium current I_{KA} and hyperpolarization-activated current I_h. For OLM neurons, it also includes calcium-activated potassium current I_{KCa} and I_h. The detailed selection of ion current in the model is based on the previously published model [32]. All neurons receive current injection to obtain baseline activity (PY: 70 pA; OLM: -10pA; BS: 2 pA). Excitatory connections between neurons include both AMPA-type and NMDA-type receptors channels, and inhibitory synaptic connections are mainly through GABA receptors. We assume that connections in the network are established based on probabilities depending on the pre-and postsynaptic cell types. According to the work of Neymotin et al. [31], we determine the connection probability and connection strength between neurons, and slightly adjust them to make neurons show physiological background state discharge in the loop.

For simplicity, similarly to previous studies [27], we assume that CA1 and CA3 neurons are modeled in the same way. The differences between CA1 and CA3 are mainly in the connections. CA3 exhibits more pronounced recurrent excitatory synaptic connections, whereas the CA1 network exhibits stronger recurrent connections between inhibitory neurons [27]. Therefore, the probability of PY-PY connection is set to 0.2 in the CA3 model and 0.05 in the CA1 model. The BS-BS connection probability and weight in the CA1 network are set to 0.55 and 4.5 nS, respectively, while the connection probability and weight in the CA3 network are set to 0.35 and 3.5 nS. Similar to CA3, all neurons receive current injections to obtain baseline activity (PY: 70 pA; OLM: -10pA; BS: 10 pA). Detailed connection parameters can be found in Appendix I.

B. The Entorhinal Cortex

Anatomical studies have shown significantly different connectivity patterns in the superficial (layers I-III) and deep (layers V and VI) layers of the EC [34]. Layer II of the EC serves as the primary output layer, providing input to the hippocampus via the perforant pathway [35]. Layer V of the EC receives the output from CA1 and subiculum [36]. The deeper layers of the EC simultaneously transmit information to the superficial layers, ensuring that hippocampal information reverts to the hippocampal-EC circuit [36], [37]. Therefore, in order to construct the complete hippocampal-EC loop, we mainly model layer II and layer V of EC. For layer II of EC we consider SC and PV interneurons. The pyramidal neurons within layer V are modeled to receive synaptic projections from CA1.

For simplicity, we assume that both PY neurons and inhibitory fast-firing neurons in the hippocampal-EC loop are modeled in the same way. Therefore, the modeling of PV neurons in layers II and V is consistent with Eq. (2), and the dynamical equations of the PY neurons in layer V are consistent with Eq. (1). The equation for SC membrane dynamics is as follows [38]:

$$C_m \frac{dV_{SC}}{dt} = -I_{Na} - I_{Nap} - I_L - I_K - I_h - I_{syn} + I_{app-SC} \tag{4}$$

where I_L, I_{Na}, I_K, I_{Nap},and I_h are the leak current, sodium current, potassium current, persistent sodium current, and hyperpolarization-activated current, respectively. The details of ion current can be found in the [38]. All neurons receive current injections to obtain baseline activity (SC:10 pA; PV of layer II: 15pA; PY: 70 pA; PV of layer V: 25pA). Specifically, SC neurons receive a slight self-excitatory projection and project to PV neurons in layer II via AMPA excitatory synapses. They also receive GABA inhibitory projections from parvalbumin (PV) interneurons. PY neurons in layer V project to SC neurons via AMPA receptors and simultaneously release excitatory information to themselves and PV neurons in layer V. PV projects to the Adend3 dendrites of PY. We assume that the EC loop contains 200 SC, 200 layer V-PY neurons, 50 layer II-PV neurons, and 50 layer V-PV neurons. The connection probabilities and connection parameters within the EC are estimated based on previous physiological studies to establish the background states [35], [39]. Detailed connection parameters can be found in Appendix I.

C. The Dentate Gyrus

For the DG region, we mainly consider GC, MC, and GABAergic interneurons (INs). GC project to IN and MC via AMPA excitatory synapses, and IN make inhibitory projections to GC and MC via GABA-type synapses. MC perform excitatory projections to GC and IN. The specific connections are shown in Fig. 1. In previous studies, the MC model is developed on the basis of the hippocampal CA3 PY model [40]. Here, we assume that the MC membrane dynamic equations follow Eq. (1), but only one somatic and one dendritic compartment are considered. The modeling of GABAergic interneurons follows Eq. (2). The somatic compartment of the GC is formulated as follows:

$$C_m \frac{dV_{GC}}{dt} = -I_{Na} - I_{Ca} - I_L - I_K - I_{SK} - I_{syn} + I_{app-GC} \tag{5}$$

where I_L, I_{Na}, I_K, I_{Ca},and I_{SK} are the leak current, sodium current, potassium current, calcium current, and calcium-dependent potassium current, respectively [51]. Similar to CA3 and EC, all neurons receive currents injection to obtain baseline activity (GC: 165 pA; IN: 50 pA; MC: 25 pA). The DG loop contains 100 GCs, 100 MCs, and 50 IN neurons. Probability-based connections between DG internal neurons, with connection probabilities and weights referenced to [26].

D. Connection Between Different Regions of the Hippocampal-EC Model

As described above, layer II of EC acts as an output layer, projecting mainly to GC neurons in DG. They also project to the Adend2 dendrites of PY neurons, BS, and OLM neurons in CA3. The soma of MC cells within the DG projects to the Adend1 dendrites of CA3. CA3 PY neurons project to the Adend2 dendrites of PY neurons in CA1 through the schaffer collateral. CA1 PY neurons project hippocampal information to the Adend2 dendrites of PY neurons in EC layer V [29]. All synaptic connections involved in the hippocampal-EC

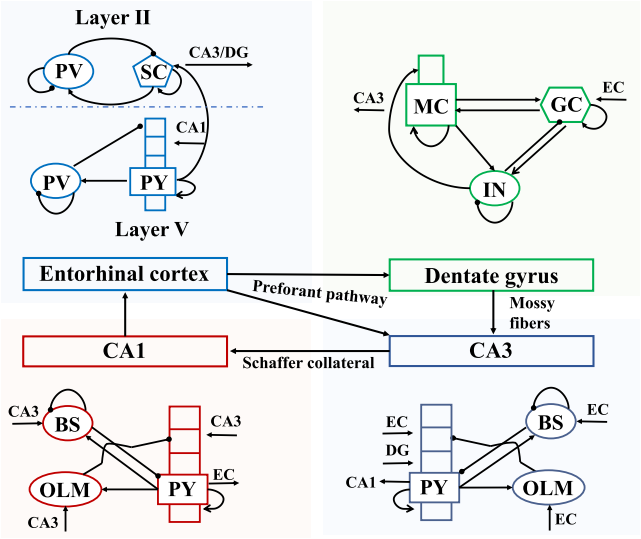

Fig. 1. Schematic of the computational model of the hippocampus-EC system. Four regions within the hippocampus, CA1, CA3, and dentate gyrus (DG), are considered. Both CA1 and CA3 contain pyramidal (PY) neurons, basket (BS) neurons, and oriens-lacunosum moleculare (OLM) neurons. PY neurons have a five-compartment structure. CA3 transmits information to all neurons in CA1 through schaffer collateral. EC is divided into layer II and layer V. Layer II is the main output layer and includes stellate cells (SC) and parvalbumin (PV) interneurons. The EC forms connections with the dentate gyrus (DG) and CA3 via the preforant pathway. Layer V is the main input layer and contains two types of neurons, PY and PV. The DG contains granule cells (GC), two-compartment mossy cells (MC), and interneurons (IN). Probabilistic connections are employed within the network, with the presence of excitatory AMPA and NMDA, and inhibitory GABA receptors. Arrows represent excitatory connections and dots represent inhibitory connections.

model used the standard NEURON biexponential mechanism. In addition, background activity is simulated by excitatory synaptic inputs, sent to the soma of all cells through Poisson processes, and used to simulate the sustained drive of other nuclei.

E. The Local Field Potential

The local field potential (LFP) signal in each electrode is derived by taking the extracellular potential contributed by each segment of each neuron. We assume that the different nuclei inside the hippocampal-EC loop are distributed inside a cylindrical volume for the insertion of LFP recording electrode positions. The cylinders are CA3, CA1, EC, and DG from top to bottom. This does not have a strict physiological meaning but is only for the calculation of the LFP potential. We use the NetPyNE to calculate the LFP of this neural population [44]. For more information on modeling LFPs see [52].

F. The Synchronization Index

We quantify the synchronization level of CA3 PY neurons using the synchronization index (SI). The specific calculation of the SI is described in the work of Pirini et al. [53]. The closer to 1 indicates a higher level of neuronal synchronization.

G. Measuring Phase-Amplitude Coupling

The modulation index (MI) mentioned by Tort et al. is used to quantify the PAC [47]. First, the original LFP signal is filtered by the EEGfilt subroutine using a linear finite impulse response (FIR) filter to obtain the required signal components for different frequency bands. Then, the number of 18 phase bins is used from 0 to 360° and the average amplitude distribution is calculated for each phase bin. The Kullback-Leibler (KL) distance is used to quantify the extent to which the amplitude distribution P in the phase-amplitude diagram deviates from the uniform distribution and indirectly reflects the magnitude of MI. More detailed PAC quantification methods are available from [47].NEURON and NetPyNE (www.neurosimlab.org/netpyne) are parallelly used to model the hippocampal-EC circuit [44]. The power spectral density analysis of LFP, the synchronization index, and the calculation of MI are performed in MATLAB.

III. Results

A. Epileptic Discharges Caused by Abnormal Excitation in the Hippocampus CA3 Region

Pyramidal cells in the hippocampal CA3 area tend to produce burst discharges under normal conditions and are easy to become pacemaker cells of epileptiform discharges. Therefore, the mechanism of epileptic discharge generated in the CA3 region is first considered. We establish the background state of the hippocampal-EC loop and then explore the effects of CA3 PY-PY AMPA synaptic connections (g_{PY-PY}) and the applied current (I_{PY}) of PY on neuronal firing properties. By changing the parameters, we find that the LFP of each region can exhibit different discharge states. Figs. 2A, 2B, 2C, and 2D show the LFP and neuronal firing raster plots at different time periods for CA3, EC, CA1, and DG, respectively. LFP of each region in the background state is displayed in 0-4s. The parameters in the background state are shown in Appendix I. In the background state, LFP shows a low-amplitude irregular firing pattern (Fig. 2). The corresponding neuronal firing raster plots in this state demonstrate a low degree of synchronization between neurons. The SI value in CA3 PY nuclei does not exceed 0.3. To analyze the changes of individual neurons in different states, we present the firing patterns of representative neurons in Fig. 3A. The PY neurons and GC in the background state show sparse firing patterns. Interneurons discharge randomly, and the discharge rate is faster than that of excitatory neurons.

To achieve excitatory hyperactivity of PY neurons, the applied current stimulation of PY neurons is increased from 70 pA to 85 pA. When the synaptic weight g_{PY-PY} is increased to 0.18 nS, the amplitude of LFP (4-8s) of CA3, CA1, EC, and DG increase. Based on the neuronal firing raster plot, the firing between neurons is clearly synchronized (Fig. 2). In this state, PY cells stimulate other cells via AMPA-mediated glutamatergic transmission and increasing the degree of synchronization of some neurons thereby triggering specific ictal events. The generated seizure events within the CA3 region are transmitted to CA1 via the Schaffer collateral and further into the EC circuits, which again affects the dynamical behavior of the hippocampal region via the DG. As the activity of CA3 PY neurons increases, the excitatory input from PY to BS increases, leading to a tendency of depolarization block in

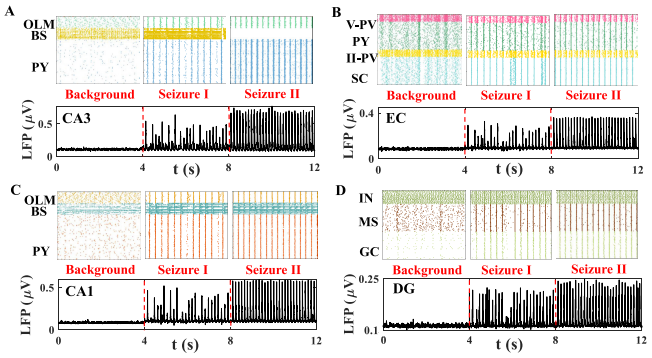

Fig. 2. Local field potential (LFP) and neural raster plots of the hippocampal-EC loop in different states. A, B, C, and D are the LFP signals and corresponding neural firing raster maps of CA3, EC, CA1, and DG, respectively. The LFP time series within 4 s are shown for each state, and the raster plot is within 2 s. In the background state, the LFP shows a low-amplitude random firing pattern, and the corresponding neural raster maps are asynchronous firing patterns. Modification of CA3 PY-PY synaptic conductance and applied current stimulation to establish the epileptic seizure I state, in which the degree of neural synchronization is increased and the corresponding LFP shows a slight increase in amplitude (I_{PY} = 85 pA, g_{PY_PY} = 0.18 nS). Continuing to increase the AMPA synaptic conductance of PY-PY within CA3 (I_{PY} = 85 pA, g_{PY_PY} = 0.20 nS), the LFP shows a clear pattern of large amplitude firing. It can be seen in the raster plots that neurons are almost completely synchronized (seizure II state).

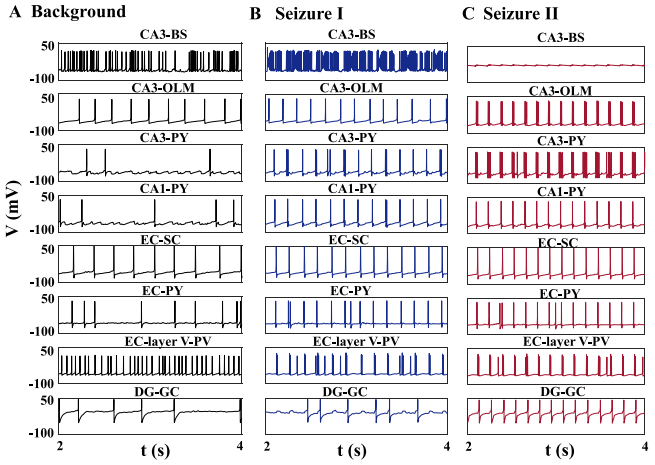

Fig. 3. Time series plots of some representative neurons in hippocampal-EC loops in A. background state, B. Seizure I state, and C. Seizure II state. Neuronal firing in the background state shows a random firing pattern, and PY neurons fire slowly. When the system transitions to the Seizure I state, CA3 BS neurons show a tendency to depolarization block due to the increased firing rate of CA3 PY neurons. In the Seizure II state, the BS neurons are completely depolarization blocked. At this time, the PY neurons show obvious regular bursting discharge patterns. The discharges within each neuron are relatively regular.

BS neurons, as shown in Fig. 3B. At the same time, the firing rate of CA3 PY neurons is significantly increased, along with the presence of irregular bursting firing pattern. The firing rates of CA1 PY neurons, SC, GC, and EC PY neurons increase, while FS neurons in layer V show bursting firing patterns. We define the state as Seizure I, where the value of SI is between 0.3 and 1 and the BS is not completely depolarization blocked.

With further increasing the g_{PY-PY} to 0.2 nS, the excitatory neurons show a fully synchronized state as shown in the raster plots (SI = 1). At this time, the LFP shows a more regular high amplitude discharge pattern (8-12s in Fig. 2). The neural discharges in the hippocampal-EC loop are obviously regular. The discharge of BS shows a complete depolarization block while that of PY neurons shows a complete bursting firing pattern (Fig. 3C). We call this state Seizure II, where SI is equal to 1, and BS neurons are completely depolarization blocked. This state is more like the status epilepticus (SE) proposed by Naze et al. [48], which is characterized by large rhythmic spikes in the 3-12 Hz band, accompanied by faster discharges in the HFO range. Therefore, we achieve the transitions of the entire hippocampal-EC loop from the background state to the two types of epileptic state by changing the synaptic connections g_{PY-PY} of CA3 and the applied current stimulus I_{PY}.

Next, we explore the HFO and PAC phenomena based on the LFP of each neural population. Fig. 4A shows the power spectral density (PSD) analysis of the LFP of the CA3 region in the three states of background, Seizure I, and Seizure II. Compared with the background state, the PSD curves of Seizure I and Seizure II have obvious peaks at 6.6 Hz and 7.3 Hz, respectively. Fig. 4B shows the results after filtering the LFP of the CA3 region. We select two frequency bands, i.e., theta band and high frequency of 100-600 Hz, to explore the coupling relationship between them. It can be seen that there is no modulation relationship between the theta band and high frequency in the background state. In the epileptic seizure states, the high-frequency amplitude is the largest at the peak and the rising edge of the low-frequency phase. Furthermore, we give the phase-amplitude comodulograms in the background, Seizure I, and Seizure II states of CA3, CA1, EC, and DG regions. The phase frequency is 1-21 Hz at the 2 Hz step and the amplitude frequency is 10-600 Hz at the 20 Hz step. For all regions, there is no significant coupling between the theta band and the HFO band in the background state.

However, in the Seizure I state, the strong coupling is observed for CA3, CA1, EC, and DG compared to the background state (warmest color in Fig. 4D). It can be seen that the coupling distribution of the amplitude frequencies within CA3 is in the range of 100-600 Hz, which contains ripples and fast ripples. In contrast, CA1, EC, and DG, which are propagation regions, have amplitude frequencies distributed around 100-400 Hz. Especially for DG and EC, the PAC phenomenon is reflected as a modulation relationship between the low frequency and ripples. Compared with the background state and Seizure I state, the coupling strength at the specific frequency band is stronger in the Seizure II state (Fig. 4E). Overall, the hippocampal- EC model can produce PAC abnormalities that correspond to the epileptogenic zone in clinical and animal experiments. Considering the origin of the HFO, the primary firing pattern of individual PY neurons still exhibits peak firing in the Seizure I state. Therefore, the HFO component within the LFP may be formed by millisecond synchronous firing within the neuron or may be provided by the rapid firing of the interneurons. In the Seizure II state, PY neurons produce bursting behavior, and the HFO of LFP

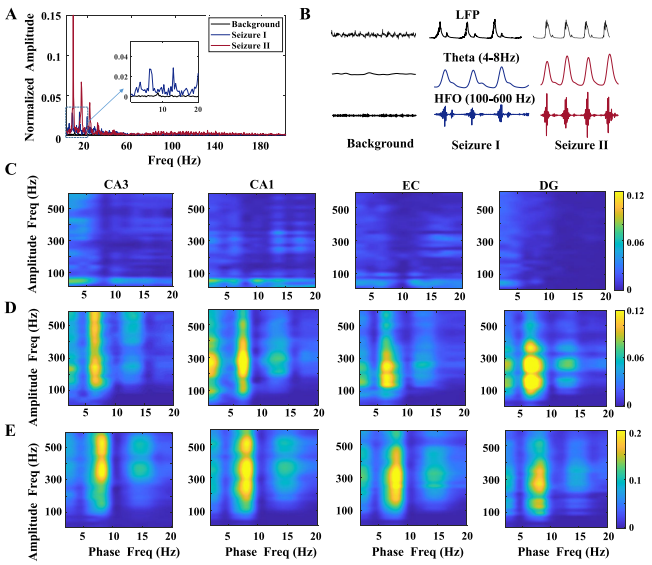

Fig. 4. Power spectral density (PSD) analysis and PAC phenomenon of LFP. A. PSD analysis plots of CA3 LFP in the background state (black), seizure I state (blue), and seizure II state (red). According to the local magnification, it can be seen that there is a clear peak of about 6.6 Hz under the Seizure I state. There is a clear peak in the seizure II state, which is about 7.3 Hz. B. According to the filtered LFP, there is no modulation between theta band and HFO in the background state. And it is obvious that the maximum amplitude of HFO is distributed in the theta phase under seizure states. C, D, and E are the phase-amplitude comodulogram of CA3, CA1, EC, and DG in the background, seizure I, and seizure II states, respectively. A strong interaction between the phase of the theta-rhythm and the amplitude of HFO can be observed in the seizure states (warmest color on each graph).

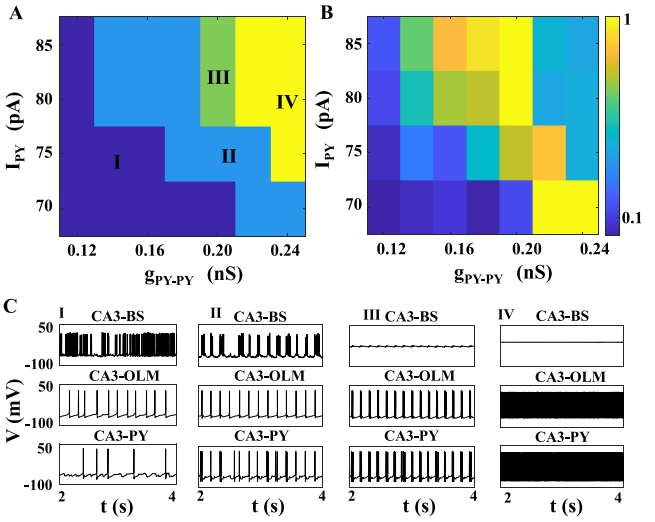

Fig. 5. The state and synchronization level analysis in the (g_{PY-PY}, I_{PY}) panel. A. The state analysis. Here the g_{PY-PY} is the AMPA synaptic conductance of CA3 PY-PY pathways. I_{PY} is the applied current stimulation of CA3 PY neurons. There are four state regions according to the range of synchronization index and discharge pattern: the background state (I), the Seizure I state (II), the Seizure II state (III), and the pathological limit state (IV). B. The synchronization level analysis in the (g_{PY-PY}, I_{PY}) panel. In region I, the synchronization index is less than 0.3. In region II, the synchronization index is distributed between 0.3-1. In region III, the synchronization index is equal to 1. In region IV, the synchronization index between neurons is maintained at about 0.4. C. The typical time series in CA3 circuits in different states. In particular, at the pathological limit state, CA3 PY and OLM neurons show high-frequency firing patterns.

may reflect the pure fast ripples characterized by single-cell behavior.

To systematically explore the transitional effects of PY-PY AMPA synaptic conductance and applied current stimulation I_{PY} on seizure-related dynamic behaviors, we present the state transition diagrams of the system at different I_{PY} and g_{PY-PY} values (Fig. 5A), as well as the corresponding synchronization level changes (Fig. 5B). According to the different firing patterns of the neurons, the whole (g_{PY-PY}, I_{PY}) panel is divided into four state areas. The synchronization index of the dark blue region does not exceed 0.3, which belongs to the asynchronous discharge state. The corresponding time series is shown in Fig. 5C, which is the background state as we defined. When I_{PY} and g_{PY-PY} increase to a certain level, the system transitions to the region II, which has a synchronization index of 0.3-1. This region corresponds to Seizure I state. In this region, BS neurons tend to depolarization block or show a depolarization block, and random bursting discharge appears in PY neurons. OLM neurons are still in peak firing mode, and the firing rate is increased.

Further increasing the excitability of CA3, the BS is completely depolarization blocked, and PY neurons and OLM neurons show a regular bursting discharge pattern. At this time, the synchronization index is 1, which corresponds to seizure II state. Notably, when further increasing g_{PY-PY} or I_{PY}, the PY neuron shows completely high-frequency firing, and the BS neuron is also completely depolarization blocked. Region IV differs from region III in that OLM neurons, have a significantly increased firing rate driven by PY. In region III, PY neurons show a distinct bursting firing pattern under the influence of inhibitory input from OLM neurons. In region IV, excitatory interactions between PYs or applied current stimulation are dominant for neural firing, resulting in a significant increase in OLM neuronal firing as well. This state is also called sustained ictal activity or pathological limit state in some studies [49], [50]. In this state, the synchronization index between neurons is maintained at about 0.4. Therefore, our study shows that enhanced excitability of PY neurons in CA3 can alter the level of synchronization between neurons, and cause the LFP to exhibit different oscillatory patterns.

B. Epileptic Discharges Caused by Increased Synapses in Mossy Cells

The MC within the DG is thought to play a key role in the onset and propagation of TLE. In a mouse model of epilepsy, an increased excitatory projection of MC to GC is found under pathological conditions [8]. In addition, the neural signal projections from the DG to the CA3 region are particularly important and play a crucial role in the generation and transmigration of TLE [28]. To investigate the excitatory and epileptogenic effect of mossy fiber, we systematically explore the effect of mossy cell synapse on the dynamic behavior of the hippocampal-EC loop by changing the synaptic weights of MC to GC and CA3 PY neurons (Fig. 6A). Fig. 6B shows the CA3 PY neuronal synchronization index in the (g_{MC-PY}, g_{MC-GC}) panel. Similar to section III-A, we divide

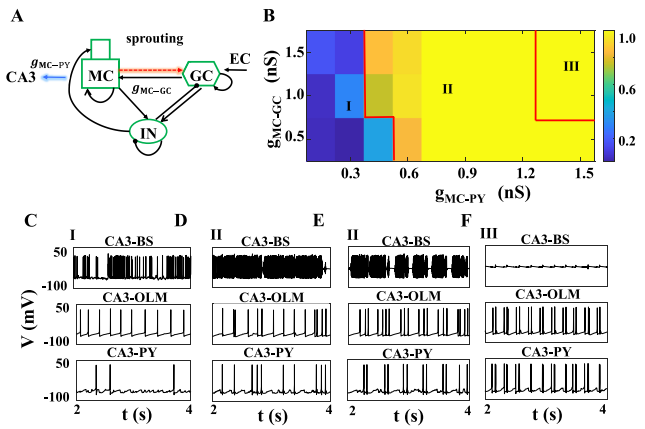

Fig. 6. The different firing states presented by PY neurons in CA3 induced by increased synapses in mossy cells. A. We consider the combined effect of MC on GC synaptic connections (red arrows) and on CA3 PY (blue arrows). B. The horizontal and vertical coordinates represent the synaptic conductance of MC-CA3 PY and MC-GC pathways, respectively. The (g_{MC-PY}, g_{MC-GC}) panel shows the value of SI changes of CA3 PY neurons. Based on the neural firing pattern and SI, the plane can be divided into three parts, I: background state (SI $\leq$ 0.3), II: Seizure I state (SI $>$ 0.3, BS shows depolarization block), III: Seizure II state (SI $=$ 1, BS is complete depolarization blocked). C-D. Time series of representative CA3 BS, OLM, and PY neurons in three states. The corresponding (g_{MC-PY}, g_{MC-GC}) of C, D, E, and F are (0.15, 0.5), (0.75, 1.0), (0.75, 1.5), and (1.35, 1.5), respectively.

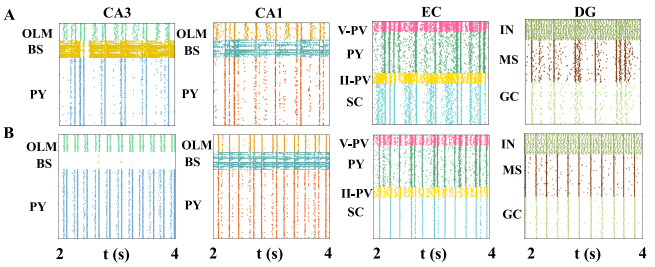

Fig. 7. Raster plots of hippocampal-EC loop neuronal firing in the Seizure I (A) and Seizure II states (B). It can be seen that the degree of neuronal synchronization is significantly increased in all populations, and in particular, the BS within CA3 is completely depolarization blocked in the Seizure II state.

the bipartite plane into background state (I), Seizure I (II), and Seizure II (III) state. According to Fig. 6B, it is found that the system can transit from the background state to the seizure I state when only the MC-PY synaptic connections are increased, i.e., $g_{MC-GC} = 0.5$. Moreover, the enhancement of MC-GC channel can promote the transition of the system from the seizure I to the seizure II state. As mentioned in previous studies, the DG itself does not produce endogenous epileptic discharges, but under pathological conditions, the epileptiform discharges of some neurons can be continuously amplified by sprouting mossy fibers. Figs. 6C-6F show the representative firing time series of BS, OLM, and PY neurons in CA3 under different states. Fig. 6C is the discharge pattern of the background state ((g_{MC-PY}, g_{MC-GC}) = (0.15, 0.5). Fig. 6D and Fig. 6E show the time series of ((g_{MC-PY}, g_{MC-GC}) at (0.75, 1.0) and (0.75, 1.5), respectively. The proportion of depolarization block in BS neurons increases with the increase of parameter values. Eventually, the BS exhibits a full depolarization block state. OLM neurons and PY neurons exhibit bursting firing patterns. The firing raster plots of neurons in the Seizure I and Seizure II states are given in Fig. 7. In particular, the biggest difference between Seizure I and Seizure II is mainly focused on the BS neurons within CA3. A high level of synchronization can be exhibited in both states. The hippocampus-EC system shows proximal synchronization within the nuclei and distal synchronization between the nuclei. Compared with the Seizure I state, in the Seizure II state, the neurons fire more regularly, and the frequency of the bursting firing is higher.

In Fig. 8A, the LFP time series diagrams of the seizure states in the hippocampus-EC system are displayed. It can be seen that in Seizure I and Seizure II states, the LFP amplitude increases and there are clear spikes, which are caused by neuronal synchronization. Further, we analyze the PAC phenomenon produced by the hyperexcitability of mossy fibers. PSD analysis of LFP in each region shows that there are significant peaks in the delta band of about 3 Hz in the seizure I state. Fig. 8B gives the phase-amplitude comodulograms of CA3, CA1, EC, and DG regions. In order to clearly observe the PAC phenomenon in each region, here we do not have a uniform colormap. It can be seen that the coupling distribution of the amplitude frequencies is in the range of 100-300 Hz. Therefore, there is a PAC phenomenon of delta modulation ripples in the Seizure I state. In the Seizure II state, PSD analysis of LFP in each region shows that there are significant peaks in the theta band of about 5 Hz. The MI indices of all regions in the Seizure II state are higher than those in the Seizure I and background states. The low frequency involved in the PAC phenomenon is mainly concentrated around 5 Hz, the high frequency of CA3 and CA1 is concentrated in 100-400Hz, while the high frequency of EC and DG is more concentrated in 100-350Hz. In particular, the CA3 region produces a more pronounced PAC phenomenon, which indirectly suggests that CA3 is more likely to be a pacemaker cell for epileptiform discharges. Therefore, mossy fiber enhancement causes epileptiform activity in the hippocampal-EC loop, which likewise produces the PAC phenomenon of low-frequency modulated HFO in different regions.

C. The Entorhinal Cortex as a Generator of Epileptic Discharges

Spontaneous seizures are recorded in both the hippocampus and EC. Previous studies have shown that in patients and models of TLE, the hyperexcitable EC may transmit excessive, synchronized, excitatory synaptic inputs to the DG. It has been reported that neurons in layer II of the EC are hyper-excited in a chronic model of TLE [42], [43]. Therefore, we focus our study on SC neurons in layer II and explore the possible role of SC-SC synaptic connections and applied currents to the SC in seizures.

We further perform two-dimensional state analysis in the (I_{SC}, g_{SC-SC}) panel. As shown in Fig. 9A, the whole (I_{SC}, g_{SC-SC}) panel can be divided into two state regions according to the degree of synchronization and firing pattern of neurons. Unsurprisingly, we find that the hippocampal-EC

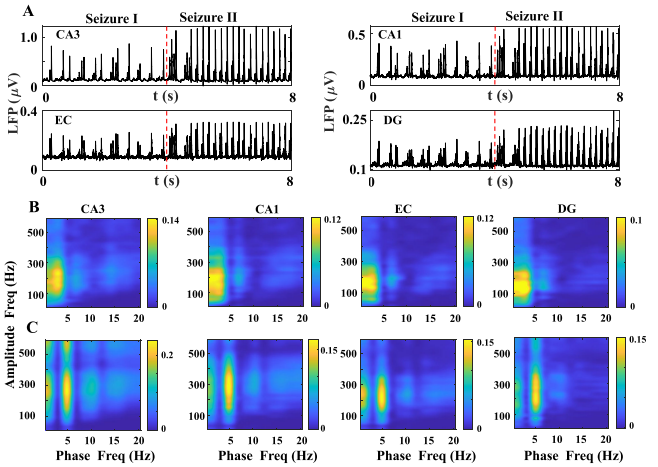

Fig. 8. LFP and PAC phenomena in different regions within the hippocampus-EC circuits. A. LFPs of CA3, CA1, EC, and DG in two seizure states. B. The phase-amplitude comodulograms of CA3, CA1, EC, and DG in the seizure I state. A strong interaction between the phase of the delta-rhythm and the amplitude of HFO can be observed in the seizure I state (warmest color on each graph). C. B. The phase-amplitude comodulograms of CA3, CA1, EC, and DG in the Seizure II state. A strong interaction between the phase of the theta-rhythm and the amplitude of HFO can be observed in the Seizure II state (warmest color on each graph).

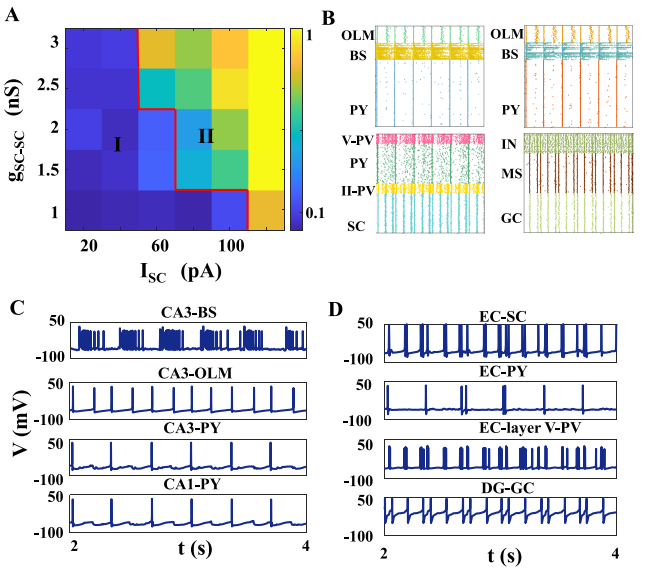

Fig. 9. The different firing states presented by PY neurons in CA3 induced by abnormal excitability of the SC. A. The panel shows the synchronous index changes of CA3 PY neurons. Based on the neural firing pattern, the plane can be divided into three parts, I: background state (SI $\leq$ 0.3), II: Seizure I state (SI $>$ 0.3). Here the g_{SC-SC} is the AMPA synaptic conductance of SC-SC pathways. I_{SC} is the applied current stimulation of SC neurons. B Raster plots of hippocampal-EC loop neuronal firing in the Seizure I states. It can be seen that the degree of neuronal synchronization is significantly increased in all populations. C. Time series plots of some representative neurons in hippocampal-EC loops.

system produces epileptic seizure when the excitability of SCs increases. It is worth noting that abnormal discharges generated by the EC only produce Seizure I state. Continuing to increase the synaptic connectivity of the SC or the applied current causes the SC to converge to a high-frequency discharge pattern. The abnormal input provided by SC, although causing PY synchronization within CA3, is not sufficient to make the BS neurons complete depolarization blocked. To visualize neuronal firing in the epileptic seizure state, a raster map of neuronal firing within the hippocampal-EC system is given in Fig. 9B ($I_{SC} = 120$, $g_{SC-SC} = 3$). It can be seen that when g_{SC-SC} and I_{SC} gradually increase, the neurons within the EC loop show a high level of synchronization and influence the firing pattern of GC through the perforant pathway. Therefore, a trend of remote synchronous discharge between GC and SC can be found. The enhanced input from GC and EC to CA3 leads to a synchronous discharge pattern within CA3. Furthermore, CA3 affects CA1 firing via schaffer collateral, which in turn eventually affects layer V pyramidal neurons of the EC.

We continue to analyze the LFP and the corresponding PAC phenomena in the seizure state caused by EC. The LFPs in the CA3 background state and Seizure I state are given in Fig. 10A. The seizure state exhibits large amplitude and regular rhythmic oscillations. The PSD curves in the epileptic seizure state have a peak at about 3 Hz. The phase-amplitude comodulograms of CA3, CA1, EC, and DG regions in the Seizure I state are given in Figs. 10C, D, E, and F, respectively. To observe the PAC phenomenon in each region, here we do not have a uniform colormap. The MI indices of all regions in the Seizure I state are higher than those in the background states. The low frequency involved in the PAC phenomenon is mainly concentrated around 1-5Hz, the high frequency of CA3

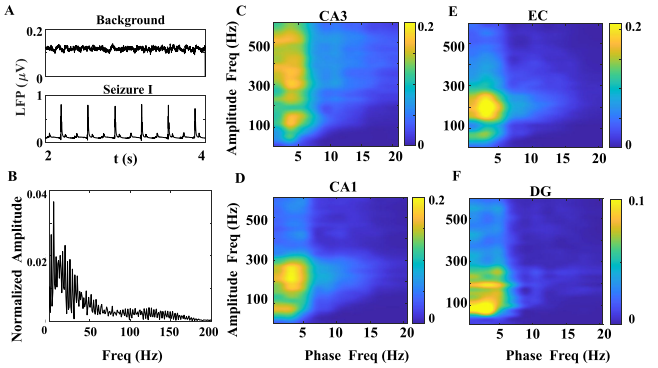

Fig. 10. LFP and PAC phenomena in different regions within the hippocampus-EC circuits. A. CA3 LFP in the background state and Seizure I states. The values of the background state parameters are consistent with those in Fig. 1, and the ISE and SE states correspond to $g_{SC-SC} = 3$, $I_{SC} = 120$ pA. B. The PSD analysis plots of CA3 LFP in the Seizure state. The first peak of the PSD curve is about 3 Hz. C-F. The phase-amplitude comodulogram of CA3, CA1, EC, and DG in the Seizure I states, respectively. A strong interaction between the phase of the 1-5Hz and the amplitude of HFO can be observed in the Seizure I states (warmest color on each graph).

is concentrated in 100-600Hz, while CA1, EC, and DG are more concentrated in 100-300Hz. Thus, abnormal excitability of the SC leads to a modulated relationship between low-frequency oscillations and ripples in EC, CA1, and DG regions of the hippocampus-EC loop. In particular, a strong coupling between low-frequency oscillations and fast ripples is also generated within CA3. Therefore, EC can act as a separate source of seizure propagation, which can lead to an abnormal

synchronous discharge pattern within the EC loop and transmit excessive, synchronous, excitatory synaptic input to the entire hippocampal-EC loop.

IV. Discussion and Conclusion

We develop a neuronal network dynamic model of the hippocampal-EC circuit to investigate the mechanism of seizure generation. We find that epilepsy is closely associated with abnormal excitation of different circuits. The simulate results explain the possible role of anatomical alterations in hippocampal-EC micro circuitry during TLE. First, our results show that increasing the self-excited connectivity of CA3 causes local neuronal synchronization that can produce specific seizure events. This result is consistent with previous modeling results [25], where CA3 axons in epilepsy patients significantly sprouted and formed dense CA3 - CA3 excitatory connections [4]. At the same time, it induces a synchronized state throughout the hippocampal-EC loop. Specifically, through simulations, we show that the system can transition from a background state to different types of seizures by enhancing the PY-PY channel within CA3 and applied current. In the Seizure I state, the degree of neuronal synchronization increases significantly, the LFP shows irregular large amplitude oscillations. BS neurons tend to depolarization block or show depolarization block. Continuing to increase the relevant parameters of CA3 again can cause the system to enter the Seizure II state, where the BS neurons are completely depolarization blocked, and the PY neurons show a regular bursting firing pattern. The LFP signals of Seizure II have a larger amplitude and more regular discharge than that of Seizure I. For neuronal populations, the Seizure II state is fully synchronized with neuronal firing. In addition, we also analyze the PAC phenomena of low-frequency modulated ripples and fast ripples in seizure states. We find that coupling between theta band and 100-600 Hz occurs within CA3 when epilepsy is generated in the CA3 region. While EC and DG appear as epileptic propagation areas with theta and 100-400 Hz PAC phenomena. The intensity of PAC was significantly stronger under Seizure II than under Seizure I. Therefore, it is likely that PAC intensity can respond to the extent of seizures. In the Seizure I state, PY neurons are in a single peak firing pattern, so it is impossible for a single neuron in PY to produce the HFO component. Thus, we suggest that the HFO may originate from millisecond synchronous firing within the PY neurons or the contribution of BS interneurons. While in the Seizure II state, the HFO within the LFP is likely to arise from high-frequency firing within the bursting of PY neurons. We further perform PAC analysis on the time series of individual neurons and find that there is also a modulation relationship between HFO and low frequency. Therefore, in the Seizure II state, HFO can also reflect the dynamic behavior of individual neurons.

In addition, the role of MCs in modulating excitation or inhibition in the DG network under pathological conditions remains controversial [5], [54]. we further explore the effect of MC neuron synaptic enhancement within the DG on epilepsy generation. We find that increasing synaptic conductance of MC-GC and MC-CA3 PY can drive the system to transition from a background state to different types of epileptic state. Under this mechanism, various regions of Seizure I exhibit mainly a modulatory relationship between ripples and delta rhythm around 2Hz. While in the Seizure II state, each region exhibits a PAC between the theta rhythm around 5 Hz and the HFO. Moreover, the PAC phenomenon is generally stronger in the Seizure II state than in the Seizure I state. The values of SI in different seizure states may be the same. Therefore, PAC phenomena reflect more features of seizure status and can provide markers for feedback stimulation. Finally, we also analyze the possible role of EC loops in seizures and focus on the hyperactivation of layer II SC neurons. Previous studies have shown recurrent excitation of layer II SCs in slices from epileptic rats [55]. In addition, spontaneous inhibitory postsynaptic currents were reduced in layer II neurons [43]. In fact, we find that increased self-excitability of SC neurons can likewise lead to changes in neuronal firing patterns that affect hippocampal loops to produce epileptic discharges. Increasing SC-SC synapses and I_{SC} leads to a transition of the system from the background state to the Seizure I state. The degree of neuronal synchronization increases significantly in the Seizure I case. Continuing to increase the parameters does not cause the system to transition to the Seizure II state, but rather drives the SC neurons to exhibit a high-frequency firing pattern. The above studies explore the possible dynamical mechanisms of TLE from different perspectives and highlight that seizures are the result of a complex network of actions. Further, interventions targeting specific nodes in the network can change their dynamics. Therefore, in subsequent studies, the regulation of epileptic activity can also be further explored based on this model and provide new therapeutic approaches.

Although the hippocampus-EC loop model can reproduce some features of TLE, it still remains limited. The limitations of this model and possible extensions in future studies need to be further discussed. First, the model does not consider the critical role of other important nuclei such as the subiculum and amygdala, which have been shown to be important in TLE in animal experiments. The critical role of other important nuclei in the limbic system should be further considered in subsequent studies. Secondly, we only consider layer II and layer V in EC. However, the cell loss in the layer III of the EC has also been demonstrated. We will continue to consider the importance of EC in subsequent studies. Moreover, the model does not consider NMDA receptors for the synaptic connections except for CA3 and CA1 circuits but focuses on the effect of AMPA synaptic conductance. Alterations in NMDA-type synaptic coupling can also achieve a dynamic transition process from interictal to ictal phases in TLE, and therefore the combined effect of different types of glutamatergic synapses on TLE will be considered subsequently. In conclusion, we perform mechanistic studies and systematically investigate the detailed role of abnormal excitability in CA3, DG, and EC on TLE. The study in this paper proposes the possible mechanisms of TLE pathogenesis from the hippocampal-EC loop system, further contributing to a comprehensive understanding of TLE pathogenesis.

REFERENCES

[1] S. S. Spencer and D. D. Spencer, "Entorhinal-hippocampal interactions in medial temporal lobe epilepsy," *Epilepsia*, vol. 35, no. 4, pp. 721–727, Jul. 1994, doi: 10.1111/j.1528-1157.1994.tb02502.x.

[2] J. Engel, "Report of the ILAE classification core group," *Epilepsia*, vol. 47, no. 9, pp. 1558–1568, Sep. 2006, doi: 10.1111/j.1528-1167.2006.00215.x.

[3] M. Avoli et al., "Network and pharmacological mechanisms leading to epileptiform synchronization in the limbic system in vitro," *Prog. Neurobiol.*, vol. 68, no. 3, pp. 167–207, Oct. 2002, doi: 10.1016/S0301-0082(02)00077-1.

[4] A. Alexander, M. Maroso, and I. Soltesz, "Organization and control of epileptic circuits in temporal lobe epilepsy," in *Prog. Brain Res.*, vol. 226, pp. 127–154, 2016, doi: 10.1016/bs.pbr.2016.04.007.

[5] P. S. Buckmaster, "Mossy fiber sprouting in the dentate gyrus," *Epilepsia*, vol. 51, p. 39, Dec. 2010, doi: 10.1111/j.1528-1167.2010.02825.x.

[6] J. Tejada and A. C. Roque, "Computational models of dentate gyrus with epilepsy-induced morphological alterations in granule cells," *Epilepsy Behav.*, vol. 38, pp. 63–70, Sep. 2014, doi: 10.1016/j.yebeh.2014.02.007.

[7] M. Diamantaki, M. Frey, P. Berens, P. Preston-Ferrer, and A. Burgalossi, "Sparse activity of identified dentate granule cells during spatial exploration," *eLife*, vol. 5, Oct. 2016, Art. no. e20252, doi: 10.7554/eLife.20252.

[8] J. J. Botterill et al., "An excitatory and epileptogenic effect of dentate gyrus mossy cells in a mouse model of epilepsy," *Cell Rep.*, vol. 29, no. 9, pp. 2875–2889, Nov. 2019, doi: 10.1016/j.celrep.2019.10.100.

[9] A. H. Siddiqui and S. A. Joseph, "CA3 axonal sprouting in kainate-induced chronic epilepsy," *Brain Res.*, vol. 1066, nos. 1–2, pp. 129–146, Dec. 2005, doi: 10.1016/j.brainres.2005.10.066.

[10] F. Du, T. Eid, E. Lothman, C. Kohler, and R. Schwarcz, "Preferential neuronal loss in layer III of the medial entorhinal cortex in rat models of temporal lobe epilepsy," *J. Neurosci.*, vol. 15, no. 10, pp. 6301–6313, Oct. 1995, doi: 10.1523/JNEUROSCI.15-10-06301.1995.

[11] C. Armstrong et al., "Target-selectivity of parvalbumin-positive interneurons in layer II of medial entorhinal cortex in normal and epileptic animals: Entorhinal cortical microcircuits and changes in epilepsy," *Hippocampus*, vol. 26, no. 6, pp. 779–793, Jun. 2016, doi: 10.1002/hipo.22559.

[12] W. W. Lytton, R. Orman, and M. Stewart, "Computer simulation of epilepsy: Implications for seizure spread and behavioral dysfunction," *Epilepsy Behav.*, vol. 7, no. 3, pp. 336–344, Nov. 2005, doi: 10.1016/j.yebeh.2005.06.011.

[13] F. Wendling, P. Benquet, F. Bartolomei, and V. Jirsa, "Computational models of epileptiform activity," *J. Neurosci. Methods*, vol. 260, pp. 233–251, Feb. 2016, doi: 10.1016/j.jneumeth.2015.03.027.

[14] M. Lévesque and M. Avoli, "High-frequency oscillations and focal seizures in epileptic rodents," *Neurobiol. Disease*, vol. 124, pp. 396–407, Apr. 2019, doi: 10.1016/j.nbd.2018.12.016.

[15] M. Lévesque, P. Salami, J. Gotman, and M. Avoli, "Two seizure-onset types reveal specific patterns of high-frequency oscillations in a model of temporal lobe epilepsy," *J. Neurosci.*, vol. 32, no. 38, pp. 13264–13272, Sep. 2012, doi: 10.1523/JNEUROSCI.5086-11.2012.

[16] E. Urrestarazu, R. Chander, F. Dubeau, and J. Gotman, "Interictal high-frequency oscillations (100–500 Hz) in the intracerebral EEG of epileptic patients," *Brain*, vol. 130, no. 9, pp. 2354–2366, Sep. 2007, doi: 10.1093/brain/awm149.

[17] H. Hashimoto et al., "Phase-amplitude coupling of ripple activities during seizure evolution with theta phase," *Clin. Neurophysiol.*, vol. 132, no. 6, pp. 1243–1253, Jun. 2021, doi: 10.1016/j.clinph.2021.03.007.

[18] X. Liu, F. Han, R. Fu, Q. Wang, and G. Luan, "Epileptogenic zone location of temporal lobe epilepsy by cross-frequency coupling analysis," *Frontiers Neurol.*, vol. 12, Nov. 2021, Art. no. 764821, doi: 10.3389/fneur.2021.764821.

[19] M. Guirgis, Y. Chinvarun, M. del Campo, P. L. Carlen, and B. L. Bardakjian, "Defining regions of interest using cross-frequency coupling in extratemporal lobe epilepsy patients," *J. Neural Eng.*, vol. 12, no. 2, Apr. 2015, Art. no. 026011, doi: 10.1088/1741-2560/12/2/026011.

[20] Y. Nonoda et al., "Interictal high-frequency oscillations generated by seizure onset and eloquent areas may be differentially coupled with different slow waves," *Clin. Neurophysiology*, vol. 127, no. 6, pp. 2489–2499, Jun. 2016, doi: 10.1016/j.clinph.2016.03.022.

[21] S. Samiee, M. Lévesque, M. Avoli, and S. Baillet, "Phase-amplitude coupling and epileptogenesis in an animal model of mesial temporal lobe epilepsy," *Neurobiol. Disease*, vol. 114, pp. 111–119, Jun. 2018, doi: 10.1016/j.nbd.2018.02.008.

[22] S. Demont-Guignard, P. Benquet, U. Gerber, and F. Wendling, "Analysis of intracerebral EEG recordings of epileptic spikes: Insights from a neural network model," *IEEE Trans. Biomed. Eng.*, vol. 56, no. 12, pp. 2782–2795, Dec. 2009, doi: 10.1109/TBME.2009.2028015.

[23] P. F. Pinsky and J. Rinzel, "Intrinsic and network rhythmogenesis in a reduced traub model for CA3 neurons," *J. Comput. Neurosci.*, vol. 1, nos. 1–2, pp. 39–60, 1994, doi: 10.1007/BF00962717.

[24] S. A. Neymotin, M. T. Lazarewicz, M. Sherif, D. Contreras, L. H. Finkel, and W. W. Lytton, "Ketamine disrupts theta modulation of gamma in a computer model of hippocampus," *J. Neurosci.*, vol. 31, no. 32, pp. 11733–11743, Aug. 2011, doi: 10.1523/JNEUROSCI.0501-11.2011.

[25] M. Sanjay and S. B. Krothapalli, "Modelling epileptic activity in hippocampal CA3," in *Hippocampal Microcircuits*, V. Cutsuridis, B. P. Graham, S. Cobb, and I. Vida, Eds. Cham, Switzerland: Springer, 2018, pp. 757–777, doi: 10.1007/978-3-319-99103-0_22.

[26] V. Santhakumar, I. Aradi, and I. Soltesz, "Role of mossy fiber sprouting and mossy cell loss in hyperexcitability: A network model of the dentate gyrus incorporating cell types and axonal topography," *J. Neurophysiology*, vol. 93, no. 1, pp. 437–453, Jan. 2005, doi: 10.1152/jn.00777.2004.

[27] J. Taxidis, S. Coombes, R. Mason, and M. R. Owen, "Modeling sharp wave-ripple complexes through a CA3-CA1 network model with chemical synapses," *Hippocampus*, vol. 22, no. 5, pp. 995–1017, May 2012, doi: 10.1002/hipo.20930.

[28] L. Zhang, D. Fan, and Q. Wang, "Transition dynamics of a dentate gyrus-CA3 neuronal network during temporal lobe epilepsy," *Frontiers Comput. Neurosci.*, vol. 11, p. 61, Jul. 2017, doi: 10.3389/fncom.2017.00061.

[29] V. Cutsuridis and P. Poirazi, "A computational study on how theta modulated inhibition can account for the long temporal Windows in the entorhinal–hippocampal loop," *Neurobiol. Learn. Memory*, vol. 120, pp. 69–83, Apr. 2015, doi: 10.1016/j.nlm.2015.02.002.

[30] S. Ahn, S. B. Jun, H. W. Lee, and S. Lee, "Computational modeling of epileptiform activities in medial temporal lobe epilepsy combined with in vitro experiments," *J. Comput. Neurosci.*, vol. 41, no. 2, pp. 207–223, Oct. 2016, doi: 10.1007/s10827-016-0614-8.

[31] S. A. Neymotin, M. M. Hilscher, T. C. Moulin, Y. Skolnick, M. T. Lazarewicz, and W. W. Lytton, "IH tunes theta/gamma oscillations and cross-frequency coupling in an in silico CA3 model," *PLoS ONE*, vol. 8, no. 10, Oct. 2013, Art. no. e76285, doi: 10.1371/journal.pone.0076285.

[32] A. B. L. Tort, H. G. Rotstein, T. Dugladze, T. Gloveli, and N. J. Kopell, "On the formation of gamma-coherent cell assemblies by oriens lacunosum-moleculare interneurons in the hippocampus," *Proc. Nat. Acad. Sci. USA*, vol. 104, no. 33, pp. 13490–13495, Aug. 2007, doi: 10.1073/pnas.0705708104.

[33] R. A. Sandler et al., "Designing patient-specific optimal neurostimulation patterns for seizure suppression," *Neural Comput.*, vol. 30, no. 5, pp. 1180–1208, May 2018, doi: 10.1162/neco_a_01075.

[34] E. S. Nilssen, T. P. Doan, M. J. Nigro, S. Ohara, and M. P. Witter, "Neurons and networks in the entorhinal cortex: A reappraisal of the lateral and medial entorhinal subdivisions mediating parallel cortical pathways," *Hippocampus*, vol. 29, no. 12, pp. 1238–1254, Dec. 2019, doi: 10.1002/hipo.23145.

[35] E. C. Fuchs, A. Neitz, R. Pinna, S. Melzer, A. Caputi, and H. Monyer, "Local and distant input controlling excitation in layer II of the medial entorhinal cortex," *Neuron*, vol. 89, no. 1, pp. 194–208, Jan. 2016, doi: 10.1016/j.neuron.2015.11.029.

[36] S. Ohara et al., "Intrinsic projections of layer Vb neurons to layers Va, III, and II in the lateral and medial entorhinal cortex of the rat," *Cell Rep.*, vol. 24, no. 1, pp. 107–116, Jul. 2018, doi: 10.1016/j.celrep.2018.06.014.

[37] J. Winterer et al., "Excitatory microcircuits within superficial layers of the medial entorhinal cortex," *Cell Rep.*, vol. 19, no. 6, pp. 1110–1116, May 2017, doi: 10.1016/j.celrep.2017.04.041.

[38] S. Middleton et al., "NMDA receptor-dependent switching between different gamma rhythm-generating microcircuits in entorhinal cortex," *Proc. Nat. Acad. Sci. USA*, vol. 105, no. 47, pp. 18572–18577, Nov. 2008, doi: 10.1073/pnas.0809302105.

[39] A. Rozov, M. Rannap, F. Lorenz, A. Nasretdinov, A. Draguhn, and A. V. Egorov, "Processing of hippocampal network activity in the receiver network of the medial entorhinal cortex layer V," *J. Neurosci.*, vol. 40, no. 44, pp. 8413–8425, Oct. 2020, doi: 10.1523/JNEUROSCI.0586-20.2020.

[40] K. Tateno, H. Hayashi, and S. Ishizuka, "Synchronized spike selection in a hippocampal dentate gyrus network model in the theta

frequency range," *Int. Congr.*, vol. 1301, pp. 79–82, Jul. 2007, doi: 10.1016/j.ics.2006.12.027.

[41] K. Geng et al., "Mechanism-based and input-output modeling of the key neuronal connections and signal transformations in the CA3-CA1 regions of the hippocampus," *Neural Comput.*, vol. 30, no. 1, pp. 149–183, Jan. 2018, doi: 10.1162/neco_a_01031.

[42] J. Bear, N. B. Fountain, and E. W. Lothman, "Responses of the superficial entorhinal cortex in vitro in slices from naive and chronically epileptic rats," *J. Neurophysiology*, vol. 76, no. 5, pp. 2928–2940, Nov. 1996, doi: 10.1152/jn.1996.76.5.2928.

[43] M. Kobayashi, X. Wen, and P. S. Buckmaster, "Reduced inhibition and increased output of layer II neurons in the medial entorhinal cortex in a model of temporal lobe epilepsy," *J. Neurosci.*, vol. 23, no. 24, pp. 8471–8479, Sep. 2003, doi: 10.1523/JNEUROSCI.23-24-08471.2003.

[44] S. Dura-Bernal et al., "NetPyNE, a tool for data-driven multiscale modeling of brain circuits," *eLife*, vol. 8, Apr. 2019, Art. no. e44494, doi: 10.7554/eLife.44494.

[45] J. Dyhrfjeld-Johnsen, V. Santhakumar, R. J. Morgan, R. Huerta, L. Tsimring, and I. Soltesz, "Topological determinants of epileptogenesis in large-scale structural and functional models of the dentate gyrus derived from experimental data," *J. Neurophysiology*, vol. 97, no. 2, pp. 1566–1587, Feb. 2007, doi: 10.1152/jn.00950.2006.

[46] R. J. Morgan and I. Soltesz, "Nonrandom connectivity of the epileptic dentate gyrus predicts a major role for neuronal hubs in seizures," *Proc. Nat. Acad. Sci. USA*, vol. 105, no. 16, pp. 6179–6184, Apr. 2008, doi: 10.1073/pnas.0801372105.

[47] A. B. L. Tort, R. Komorowski, H. Eichenbaum, and N. Kopell, "Measuring phase-amplitude coupling between neuronal oscillations of different frequencies," *J. Neurophysiol.*, vol. 104, no. 2, pp. 1195–1210, 2010, doi: 10.1152/jn.00106.2010.

[48] S. Naze, C. Bernard, and V. Jirsa, "Computational modeling of seizure dynamics using coupled neuronal networks: Factors shaping epileptiform activity," *PLOS Comput. Biol.*, vol. 11, no. 5, May 2015, Art. no. e1004209, doi: 10.1371/journal.pcbi.1004209.

[49] D. Depannemaecker, A. Ivanov, D. Lillo, L. Spek, C. Bernard, and V. Jirsa, "A unified physiological framework of transitions between seizures, sustained ictal activity and depolarization block at the single neuron level," *J. Comput. Neurosci.*, vol. 50, no. 1, pp. 33–49, Feb. 2022, doi: 10.1007/s10827-022-00811-1.

[50] M. Du, J. Li, R. Wang, and Y. Wu, "The influence of potassium concentration on epileptic seizures in a coupled neuronal model in the hippocampus," *Cognit. Neurodynamics*, vol. 10, no. 5, pp. 405–414, Oct. 2016, doi: 10.1007/s11571-016-9390-4.

[51] G. L. F. Yuen and D. Durand, "Reconstruction of hippocampal granule cell electrophysiology by computer simulation," *Neuroscience*, vol. 41, nos. 2–3, pp. 411–423, Jan. 1991, doi: 10.1016/0306-4522(91)90337-N.

[52] H. Parasuram, B. Nair, E. D'Angelo, M. Hines, G. Naldi, and S. Diwakar, "Computational modeling of single neuron extracellular electric potentials and network local field potentials using LFPsim," *Frontiers Comput. Neurosci.*, vol. 10, Jun. 2016, doi: 10.3389/fncom.2016.00065.

[53] M. Pirini, L. Rocchi, M. Sensi, and L. Chiari, "A computational modelling approach to investigate different targets in deep brain stimulation for Parkinson's disease," *J. Comput. Neurosci.*, vol. 26, no. 1, pp. 91–107, Feb. 2009, doi: 10.1007/s10827-008-0100-z.

[54] A. Kecskés, B. Czéh, and M. Kecskés, "Mossy cells of the dentate gyrus: Drivers or inhibitors of epileptic seizures?" *Biochimica et Biophysica Acta (BBA) - Mol. Cell Res.*, vol. 1869, no. 9, Sep. 2022, Art. no. 119279, doi: 10.1016/j.bbamcr.2022.119279.

[55] S. S. Kumar, X. Jin, P. S. Buckmaster, and J. R. Huguenard, "Recurrent circuits in layer II of medial entorhinal cortex in a model of temporal lobe epilepsy," *J. Neurosci.*, vol. 27, no. 6, pp. 1239–1246, Feb. 2007, doi: 10.1523/JNEUROSCI.3182-06.2007.